LAWRENCE
LIVERMORE
NATIONAL
LABORATORY

UCRL-CONF-222482

On the Nature of Variations in Density and Composition within TATB-based Plastic Bonded Explosives

J. H. Kinney, T. M. Willey, G. Overturf

June 28, 2006

Detonation Symposium
Norfolk, VA, United States
July 23, 2006 through July 28, 2006

ON THE NATURE OF VARIATIONS IN DENSITY AND COMPOSITION WITHIN TATB-BASED PLASTIC BONDED EXPLOSIVES

John H. Kinney*, Trevor M. Willey*, George E. Overturf*
*Lawrence Livermore National Laboratory
Livermore, CA 94550

Initiation of insensitive high explosives is affected by porosity in the 100 nm to micron size range. It is also recognized that as-pressed plastic bonded explosives (PBX) are heterogeneous in composition and density at much coarser length scale (10 microns – 100 microns). However, variations in density and composition of these explosives have been poorly characterized. Here, we characterize the natural variations in composition and density of TATB-based PBX LX-17 with synchrotron radiation tomography and ultra small angle x-ray scattering. Large scale variations in composition occur as a result of binder enrichment at the prill particle boundaries. The pore fraction is twice as high in the prill particle as in the boundary. The pore distribution is bimodal, with small pores of 50-100 nm in radius and a broader distribution of pores in the 0.5 – 1.5 micron size range. The higher pore density within the prill particle is attributed to contact asperities between the crystallites that might inhibit complete consolidation and binder infiltration.

INTRODUCTION

Plastic bonded explosives (PBX) consist of explosive crystals dispersed in a polymeric binder. One such PBX, the insensitive high explosive LX-17, is formed from the water dispersion of TATB crystallites (1,3,5-triamino-2,4,6-trinitrobenzene), with the subsequent slurry mixing with the solvated polymeric binder Kel-F-800. With solvent evaporation, the Kel-F coated TATB crystallites clump into prill particles of varying sizes. The prill particles are then consolidated at high pressure to form a finished explosive of uniform density and composition.

The sensitivity of high explosives depends on formation of "hot-spots." When shocked to high pressures,[1] these small regions of localized thermal energy sustain and propagate a detonation event; it is believed that pores present within the explosive give rise to these hot-spots. Detonation properties, especially of insensitive explosives such as TATB, depend particularly on the size and spatial uniformity of these hot-spots.[2, 3] Thus, inhomogeneous distribution of either TATB crystallites or porosity in PBX will affect their shock sensitivity.[4-6]

X-ray radiographs of pressed LX-17 explosives display a characteristic prill texture. As x-rays are sensitive to chemical composition and density, this radiographic texture reflects variations in composition and/or density in the explosive. Because heterogeneities in the microstructure can affect detonation properties, it is important to understand the origin of the prill texture in terms of the microstructure.

Here, we utilize the techniques of multiple-energy synchrotron radiation computed tomography (SRCT) and ultra-small angle x-ray scattering (USAXS) to fully characterize as-pressed specimens of LX-17 PBX. The SCRT provides a three-dimensional mapping variations in composition and density within the PBX with better than 10 micron spatial resolution. The USAXS provides the size distribution of pores in the nanometer to micron size range.

EXPERIMENTAL METHODS

Specimens of LX-17 were prepared with 92.5 wt% TATB and 7.5 wt% Kel-F 800 binder. The median TATB particle size was 35 microns. Control specimens (specimens without the Kel-f 800 binder) were also prepared from ultra-fine TATB, which was 99.95% TATB. The median particle size of TATB used in the controls was approximately 7 microns.

For the SRCT measurements, a formulation of 92.5 wt% TATB and 7.5 wt% Kel-F 800 binder were pressed isostaticlly at 2.07 x 10^5 kPa for 5 minutes at 100C to a dimension of 15mm diameter by approximately 2.5 cm length (see Figure 1). The density of the pellet was measured gravimetrically, and determined to have a density (to three figures) of 1.914 g/cc.

The specimen was mounted to a rotating stage, and scanned with the tomography apparatus on beamline 10-2 at the Stanford Synchrotron Radiation Facility at 0.5 degree rotational increments through 180 degrees (360 views of the specimen). Scans were obtained at x-ray energies of 17, 19.5, 25, and 30 keV. Monochromatic energies were selected by rotation of a double crystal Si monochromator operated in the (220) reflection. The monochromator was detuned off of the rocking curve maximum to eliminate possible harmonic contamination.

Three-dimensional reconstructions of the data were obtained with Fourier-filtered backprojection. Image reconstruction provided a complete, three-dimensional mapping of the average linear x-ray attenuation coefficient within a 9 micron cube at each location within the specimen. The linear attenuation coefficient α (in units of cm-1) is related to the composition and density of the specimen:[7, 8]

$$\alpha_m = \sum_i \alpha_i V_i \qquad (1)$$

In equation 1, V_i are the volume fractions of the constituents (TATB, Kel-F, and pores) subject to the constraints that V_i sum to one, and the α_i are the linear x-ray attenuation coefficients of the constituents. The linear attenuation coefficients are calculated from tabulated mass attenuation coefficients and known physical density of pure TATB and Kel-F binder.[9]

Specimens were prepared in a similar fashion for USAXS measurements. For these measurements, cylindrical pellets, nominally 0.8 mm thick by 10 mm in diameter were pressed as above, with the singular exception that the ultrafine control specimen was pressed at 25C. Pellet densities were determined geometrically using the measured thickness, the die radius, and the weight of each sample.

The USAXS specimens were scanned at the UNICAT beamline 33-ID at the Advanced Photon Source, Argonne National Laboratory. The scanning was performed with a Bonse-Hart camera,[10] which can measure scattering vectors (q) from about 0.001-10 nm^{-1}. The scanning energy was 10.97 keV. Data were processed using the codes developed for the beamline, and included absolute scattering intensity calibration and slit desmearing.[11] The maximum entropy method, implemented in the "Irena" package for SAS data analysis, was used to determine the pore size distribution within the specimens.[12]

EXPERIMENTAL RESULTS

Synchrotron radiation microCT

A representative SRCT cross-section of the specimen is shown in Figure 1. The characteristic "prill" texture is apparent in this slice; the lattice-like structure (lighter colors) is the boundary between the prill particles (darker colors). The x-ray attenuation is greatest in the prill boundaries. From the measured attenuation coefficients, it is possible to obtain the volume fractions of each constituent in a representative volume element (in this case, cubic elements 9 microns on edge), provided that we have accurate values for the mass attenuation coefficients of each constituent. Absent a calibration standard, it is necessary to calculate these coefficients from tables of mass attenuation coefficients of the elements. By necessity, this is the approach taken here.

The calculated x-ray attenuation coefficients (solid line) are compared with the SRCT measurements (solid circles) at four different x-ray energies. Within experimental uncertainty (<0.1%), measured and calculated values are identical. For example, at 19.5 keV, both the measured and calculated values of the linear attenuation coefficient were 1.54 cm^{-1}. This close correspondence indicates that the tabulated mass attenuation coefficients are accurate within the energy range used in this study.

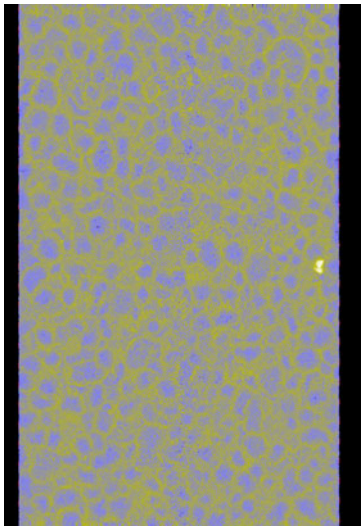

Figure 1: A 9-micron thick SRCT section through LX-17. The lighter colored web-like structures are the prill boundaries; the darker colored regions are the prill particles. Variations in colorization reflect variations in composition and density.

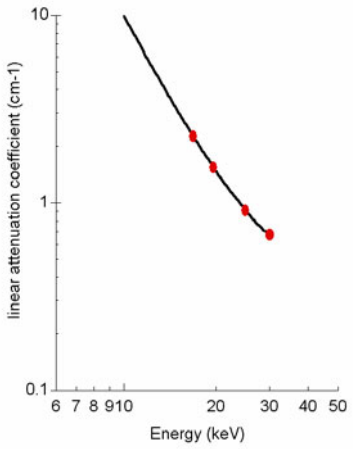

Figure 2. Calculated mean linear attenuation coefficient of LX-17 using the tabulated mass attenuation coefficients and measured density of the explosive (solid line) with the linear attenuation coefficients measured by CT (solid circles). The close correspondence of the measured and calculated values (within 0.1% at all energies) provides confidence in the tabulated coefficients used in this study.

The 3D SRCT images were segmented into boundary and particle phases. The mean values of the linear attenuation coefficients were determined for both phases at 19.5 and 25 keV. Solving equation 1 subject to the constraint that the volume fractions of TATB, Kel-F, and porosity sum to one, the volume fractions of each constituent could be determined uniquely in both the boundary phase and prill particle. These results are tabulated in Table 1.

USAXS

The USAXS data were analyzed assuming dilute pore concentration with uncorrelated positions and random orientations. The angular dependence of the scattered radiation was approximated as:[13]

$$I(Q) = |\Delta\rho|^2 \int_0^\infty \left| F(Q,r)^2 V^2(r) NP(r) dr \right| \quad (2)$$

In Equation 2, Q is the magnitude of the scattering vector, r is the size of the pore, $\Delta\rho$ is the difference in electron density between the pore and the solid, $F(Q,r)$ is the scattering form factor, $V(r)$ is the volume of the pore, N is the total number of pores, and $P(r)$ is the probability of having a pore of size r. The size distribution was calculated assuming a spherical form factor, using an iterative curve fitting to the scattering data.

Void size distributions in typical specimens of LX-17 and ultra-fine are graphed in Figure 3 top and bottom. The pore size distribution in LX-17 is bimodal, with a sharp peak centered at approximately 10nm, and a broad distribution centered at approximately 100nm. The ultra-fine also showed a beak at 10nm, but it was obscured by a prominent broad peak centered near 50nm.

The distributions were integrated to obtain the pore volume fraction for pores up to about 2 microns in diameter. For LX-17, the void volume fraction was .015 (.002), and the ultrafine averaged .036 (.005). These accounted for 60-100% of the void volume expected from the density measurements; agreement with physical density was better with specimens closer to the maximum theoretical density, indicating that some of the specimens had pores greater than 2 microns in diameter.

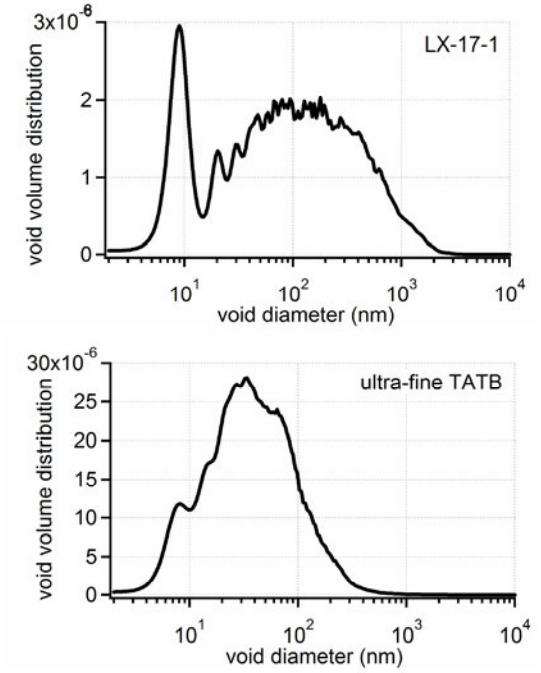

Figure 3: Top, void size distribution in a specimen of LX-17. Bottom, void size distribution in ultra-fine TATB without binder. The 10nm peak was common to both PBX and ultrafine, and is believed to represent intrinsic pores in the TATB crystallites. The larger pores are believed to be due to incomplete consolidation of the explosive during processing.

DISCUSSION

As the SRCT images and the quantitative results of Table 1 demonstrate, LX-17 is a heterogeneous structure. The heterogeneities are caused by the incomplete consolidation of the prill particles, leaving a residue structure of particles with a Kel-F – rich boundary layer. The density variations are quite small: the physical density of the boundary layer is 1.925 g/cc and the density of the particle is 1.898 g/cc. However, pore volume is almost doubled in the prill particle.

The prill texture, therefore, is due to two factors: an enrichment of Kel-F in the boundary phase, and the fact that the Kel-F binder has greater x-ray absorption than TATB. Figure 4 shows the ratio of the x-ray mass attenuation coefficients of the Kel-F and TATB over the energy range used in this study.

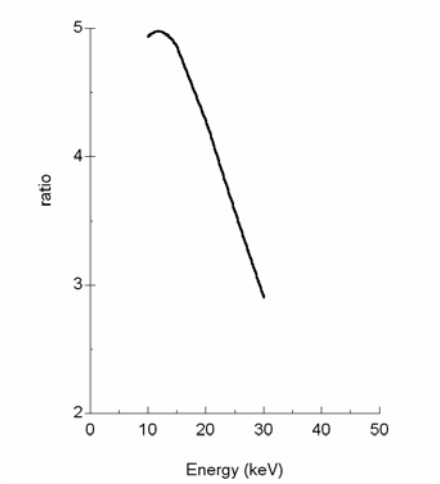

Figure 4: The ratio of the x-ray mass attenuation coefficients (Kel-F/TATB) as a function of x-ray energy. The prill texture in x-ray radiographs is a result of both enrichment of Kel-F binder at the prill boundaries and the greater x-ray attenuation of the Kel-F.

Though the SRCT images quantified the pore concentration in the LX-17 formulation, the pore size distribution could not be determined with the resolution of the x-ray CT imaging system. Therefore, USAX was used to derive the pore size distribution in the pore size range from approximately 1 nm to 2 μm. With a scattering form factor for spheres, a maximum entropy algorithm calculated the size distributions of the voids. This iterative, linear inversion method did not require an *a priori* guess as to the shape of the distribution, and converged to a unique distribution of pore sizes.

Both LX-17 and UFTATB had a bimodal distribution of pore sizes. Both formulations had a narrow peak centered between 8-10 nm in pore diameter, and a broad distribution at a larger diameter. Because of their nearly identical scattering profiles, the pores distributed around 10 nm in size were attributed to intra-crystalline voids within the TATB crystallites. The larger pores were attributed to voids between the crystallites, either at the TATB/binder interface or within the binder itself. The large pore distribution was centered at 100 nm in the LX-17 formulation, with diameters ranging from 20 nm to 2 μm. The large voids were log-normal in distribution.

Combining the information from the imaging and the USAXS, it is clear that the increased porosity in the prill particle is not due to the intra-crystalline voids in the TATB because the pore density is twice as high within the prill particle while the number of TATB crystals is increased by

only a couple percent. Therefore, we hypothesize that the increased porosity in the prill particle reflects a higher concentration of larger pores. These pores might arise from contact asperities between the crystallites that prevent more complete consolidation or binder infiltration.

In conclusion, the polymer bound explosive LX-17 is heterogeneous, as there are variations in both void concentration and composition. The texture observed in radiographs reflects these heterogeneities; there is clear evidence of binder enrichment at prill particle boundaries, and an increased concentration of large voids within the prill particles. The influence of these heterogeneities upon detonation behavior is now the focus of both experiment and modeling studies at Lawrence Livermore National Laboratory.

Table 1. Multi-energy SRCT results

location	TATB V%	KEL-F V%	porosity V%
particle	92.10	5.91	1.99
boundary	90.48	8.48	1.04

ACKNOWLEDGMENTS

The authors thank Tony van Buuren, Jon Lee, Jeff Handly, and Brandon Weeks. We also thank Jan Ilavsky and Pete Jemian of the APS. The UNICAT facility at the Advanced Photon Source (APS) is supported by the U.S. DOE under DEFG02-91ER45439, through the Frederick Seitz materials Research Laboratory at the University of Illinois at Urbana-Champaign, the Oak Ridge national laboratory (DE-AC05-00OR22725 with UT-Battelle LLC), the National Institute of Standards and Technology and UOP LLC. The APS is supported by the U.S. DOE, Basic Energy Sciences, Office of Science under contract W-31-109-ENG-38. Stanford Synchrotron Radiation Laboratory is supported by the U.S. DOE Basic Energy Sciences.

This work was performed under the auspices of the U.S. Department of Energy by the University of California Lawrence Livermore National Laboratory under Contract No. W-7405-ENG-48.

REFERENCES

1. Bowden, F. P. & Yoffe, Y. D. Initiation and growth of explosion in liquids and solids (Cambridge University Press, Cambridge, 1985).
2. Politzer, P. & Boyd, S. Structural Chemistry 13, 105-113 (2002).
3. Tarver, C. M., Chidester, S. K. & Nichols, A. L. Journal of Physical Chemistry 100, 5794-5799 (1996).
4. Field, J. E. Accounts of chemical Research 25, 489-496 (1992).
5. Hatano, T. Physical Review Letters 92, 015503 (2004).
6. Mintmire, J. W., Robertson, D. H. & White, C. T. Physical Review B 49, 14859-14864 (1994).
7. Kinney, J. H., Balooch, M., Haupt, D. L., Jr., Marshall, S. J. & Marshall, G. W., Jr. Mineral distribution and dimensional changes in human dentin during demineralization. J Dent Res 74, 1179-84 (1995).
8. Kinney, J. H. & Nichols, M. C. X-Ray Tomographic Microscopy (XTM) Using Synchrotron Radiation. Annual Review of Materials Science 22, 121-152 (1992).
9. Plechaty, E. F., Cullen, D. E. & Howerton, R. J. (Lawrence Livermore National Laboratory, Livermore California, 1981).
10. Pahl, R., Bonse, U., Pekala, R. W. & Kinney, J. H. Saxs Investigations on Organic Aerogels. Journal of Applied Crystallography 24, 771-776 (1991).
11. Ilavsky, J., Allen, A. J., Long, G. G. & Jemian, P. R. Review of Scientific Instruments 73, 1660-1662 (2002).
12. Ilavsky, J. & Jemian, P. R. in http://www.uni.aps.anl.gov/~ilavsky/irena.html (2005).
13. Roe, R. J. Methods of Xray and Neutron Scattering in Polymer Science (Oxford University Press, Oxford, 2000).